Redox Properties of the Isolated Flavin Mononucleotide- and Flavin Adenine Dinucleotide-Binding Domains of Neuronal Nitric Oxide Synthase†

Pierre E. Garnaud, Martijn Koetsier, Tobias W. B. Ost, and Simon Daff*

School of Chemistry, University of Edinburgh, King's Buildings, West Mains Road, Edinburgh EH9 3JJ, U.K.

Received April 7, 2004; Revised Manuscript Received June 15, 2004

ABSTRACT: Electron transfer through neuronal nitric oxide synthase (nNOS) is regulated by the reversible binding of calmodulin (CaM) to the reductase domain of the enzyme, the conformation of which has been shown to be dependent on the presence of substrate, NADPH. Here we report the preparation of the isolated flavin mononucleotide (FMN)-binding domain of nNOS with bound CaM and the electrochemical analysis of this and the isolated flavin adenine dinucleotide (FAD)-binding domain in the presence and absence of $NADP^+$ and ADP (an inhibitor). The FMN-binding domain was found to be stable only in the presence of bound CaM/Ca^{2+}, removal of which resulted in precipitation of the protein. The FMN formed a kinetically stabilized blue semiquinone with an oxidized/semiquinone reduction potential of −179 mV. This is 80 mV more negative than the potential of the FMN in the isolated reductase domain, that is, in the presence of the FAD-binding domain. The FMN semiquinone/hydroquinone redox couple was found to be similar in both constructs. The isolated FAD-binding domain, generated by controlled proteolysis of the reductase domain, was found to have similar FAD reduction potentials to the isolated reductase domain. Both formed a FAD−hydroquinone/$NADP^+$ charge-transfer complex with a long-wavelength absorption band centered at 780 nm. Formation of this complex resulted in thermodynamic destabilization of the FAD semiquinone relative to the hydroquinone and a 30 mV increase in the FAD semiquinone/hydroquinone reduction potential. Binding of ADP, however, had little effect. The possible role of the nicotinamide/$FADH_2$ stacking interaction in controlling electron transfer and its likely dependence on protein conformation are discussed.

Nitric oxide (NO) is produced physiologically to fulfill a range of signaling functions and as an immune response agent (*1*, *2*). The mammalian NO synthases (NOS) generate NO by catalyzing the monooxygenation of L-arginine to *N*-hydroxy-arginine and the subsequent conversion of this to citrulline (*3*, *4*). During each cycle, 2 equiv of dioxygen and 1.5 equiv of NADPH are consumed. Four cofactors are required for activity: a cysteine-ligated heme, bound by the oxygenase domain, around which the active site is constructed (*5*, *6*), tetrahydrobiopterin, an electron donor/acceptor required during oxygen activation, and one each of flavin mononucleotide (FMN) and flavin adenine dinucleotide (FAD), bound by the reductase domain. The mammalian NO synthases are homodimers with each subunit arranged such that the reductase domain of one subunit supplies the oxygenase domain of the other with electrons (*7*, *8*). There are three isoforms, two of these are constitutively expressed (neuronal, nNOS,[1] and endothelial, eNOS) and are activated by the reversible binding of calmodulin (CaM) at elevated concentrations of intracellular calcium. The third is known as the inducible isoform; it was first discovered in macrophages and binds CaM even at negligible Ca^{2+} concentrations and is regulated at the transcriptional level. The NO synthase oxygenase domain is structurally unique and forms the main dimer interface in the enzyme (*5*, *6*), whereas the reductase domain is closely related by sequence and structure to mammalian cytochrome P450 reductase (CPR) (*9*−*11*). For both CPR and NO synthase, the reductase domains are composed of a FAD-binding domain, related to ferredoxin reductase (FNR), which is fused to a FMN-binding domain, related to flavodoxin. Electrons derived from NADPH dehydrogenation at the FAD site are transferred sequentially via the FMN to the heme. The FMN oscillates between the hydroquinone and semiquinone oxidation states during catalysis and functions as a single electron donor (*12*). The FMN to heme electron transfer appears to be the critical rate-determining event for NO synthesis and is also the step activated by CaM (*13*). Electrons can also be transferred

† This work was supported by the Wellcome Trust. S.D. is a Royal Society (U.K.) University Research Fellow. P.E.G. was supported by a University of Edinburgh, School of Chemistry Christina Millar studentship. M.K. was supported by the E.U. Erasmus scheme and is currently at the Biomolecular Science & Biotechnology Institute, University of Groningen, NL-9747 AG Groningen, The Netherlands.

* Corresponding Author. Tel. +44-131-650-7378. E-mail. Simon.Daff@ed.ac.uk.

[1] Abbreviations: nNOSrd, recombinant neuronal nitric oxide synthase reductase domain; nNOS, iNOS, and eNOS, neuronal, inducible, and endothelial nitric oxide synthases; nNOSFMNCaM, the recombinant FMN-binding subdomain of rat nNOS with bound CaM; nNOSFAD, the FAD-binding subdomain of rat nNOS generated proteolytically; CPR, mammalian cytochrome P450 reductase; CaM, calmodulin; EGTA, ethylene bis(oxyethylene-nitrilo)tetraacetic acid; DTT, dithiolthreitol; PMSF, phenylmethylsulphonyl fluoride; IPTG, isopropyl-β-D-thiogalactopyranoside; OTTLE, optically transparent thin-layer electrode; sq, flavin semiquinone; hq, flavin hydroquinone; NMN, nicotinamide mononucleotide.

10.1021/bi049312v CCC: $27.50
Published on Web 08/11/2004

specifically from the FMN to the external electron acceptor, cytochrome *c*. This process was also found to be CaM-dependent in both the holoenzyme and the isolated nNOS reductase domain (*14*, *15*). The redox properties of the cofactors are largely independent of CaM, suggesting that the activation mechanism involves a structural rearrangement of the reductase domain (*16*, *17*).

The nNOS and eNOS reductase domains both contain a series of additional protein inserts/extensions, which have been shown to control their calmodulin dependence (*18*). These include the CaM binding site, which is located at the N-terminus and consists of approximately 20 amino acids, an autoinhibitory insert of 42−45 amino acids located in the middle of the FMN-binding domain (*19*−*21*), and an autoinhibitory C-terminal extension of 20−30 amino acids (*21*, *23*). The sequences of the inserts are all isoform-specific and help to define the three different enzyme groups. The autoinhibitory domains appear to suppress the reductase and NO-synthesis activity of the enzyme, and CaM binding relieves this effect. Recently the substrate, NADPH, was also shown to inhibit electron transfer from reduced nNOSrd to cytochrome *c* by stabilizing a conformation in which the FMN is inaccessible to electron acceptors (*24*). The mechanism by which NADPH exerts conformational control may involve the FAD stacking residue F1395 (*25*), which lies at the start of the autoinhibitory C-terminal extension, and may also be dependent on the redox state of the FAD.

This study focuses on the redox properties of the isolated FMN- and FAD-binding domains, particularly the effect of substrate ($NADP^+$) binding on the reduction potentials of the FAD cofactor.

EXPERIMENTAL PROCEDURES

Expression and Purification of Recombinant nNOS FMN Domain Plus Calmodulin (nNOSFMNCaM). The nNOSFMNCaM (pCRNNFMN) expression plasmid was constructed from plasmid pCRNNR, the expression plasmid for rat nNOS reductase domain (nNOSrd) residues 695−1429 (including the CaM binding site) and synthetic bovine brain calmodulin (*26*). The gene for nNOSrd was excised using *Eco*R1, and a fragment corresponding to the FMN-binding domain (residues 695−946) was amplified using PCR. The following PCR primers were used to introduce *Eco*R1 sites at either end of the sequence: 5′-gactcatgaattcatgctcaactatagactc-3′ (forward) and 5′-tcaggatccgaattctcaatcccccacgcagaac-3′ (reverse). The resultant gene fragment was cloned back into the *Eco*R1 site of the original vector in place of the nNOSrd sequence. Recombinant nNOSFMN and CaM were coexpressed in *Escherichia coli* strain JM109 (DE3) as described for nNOSrd (*26*). The cells were lysed by sonication on ice in 50 mM Tris-HCl, pH 7.5, 0.1 M KCl, and 1 mM $CaCl_2$ (buffer A) with 1 mL of protease inhibitor cocktail for non-His-tagged proteins per 30 g of *E. coli* (Sigma) and 1 mM PMSF. The lysate was centrifuged at 20 000*g* for 1 h, and the supernatant was passed through a DEAE Sepharose column (2.5 cm × 15 cm) and eluted with buffer A. The nNOSFMNCaM fractions were loaded on to a Q-Sepharose FPLC column (Pharmacia) and eluted with a gradient of 0.1−0.4 M KCl in buffer A. Enzyme-containing fractions were concentrated to approximately 100 μM and stored at −80 °C. To remove excess CaM, enzyme fractions were further purified by Superdex S200 FPLC chromatography in 50 mM Tris-HCl, pH 7.5, 0.2 M KCl, 1 μM $CaCl_2$.

Preparation of Recombinant nNOSrd and nNOS FAD Domain (nNOSFAD). Recombinant rat nNOS reductase domain residues 695−1429 (nNOSrd) and synthetic bovine brain calmodulin were expressed in *E. coli* strain JM109 (DE3) using plasmid pCRNNR (*26*) and purified as described previously on 2′,5′-ADP-agarose (Sigma) and CaM-agarose (Sigma) (*24*). nNOS FAD domain was generated by digesting 10 mL of 20 μM nNOSrd with 1 mL of immobilized trypsin (Sigma) in 50 mM Tris-HCl, pH 7.5, 0.1 M KCl, (buffer B) at room temperature for 2 h with gentle stirring (*10*). The suspension was centrifuged at 2000*g* for 10 min and filtered to remove the trypsin, and the supernatant was applied to a 2′,5′-ADP-agarose column (1 cm × 10 cm). The yellow band was washed with 100 mL of buffer B and eluted with 20 mL of 1 mM 2′,5′-ADP in buffer B plus 0.3 M KCl. Enzyme-containing fractions were concentrated to approximately 200 μM and stored at −80 °C. It should be noted that the nNOS FAD domain generated in this way is truncated by 22 amino acids from the C-terminus and consists of residues 963−1407 of rat nNOS (*10*).

Spectroelectrochemistry. Spectroelectrochemical analysis of nNOSFMNCaM, nNOSrd, and nNOSFAD was conducted in an OTTLE cell constructed from a modified quartz electron paramagnetic resonance (EPR) cell with a 0.3 mm path length containing a Pt/Rh (95/5) gauze working electrode (wire diameter 0.06 mm, mesh size 1024 cm^{-1}, Engelhardt, U.K.), a platinum wire counter electrode, and a Ag/AgCl reference electrode (model MF2052, Bioanalytical Systems, West Lafayette, IN 47906) (*27*). Enzyme samples (1 mL × 200 μM) were eluted through a G25 column preequilibrated with 0.1 M Tris pH 7.5, 0.5 M KCl, concentrated to 300 μM, and stored overnight in an anaerobic glovebox at 0 °C. The following mediators were then added: pyocyanine (10 μM), 2-hydroxy-1,4-naphthoquinone (20 μM), FMN (5 μM), benzyl viologen (10 μM), and methyl viologen (10 μM). Spectroelectrochemical titrations were performed at 25 ± 2 °C using an Autolab PGSTAT10 potentiostat and a Cary 50 UV/vis spectrophotometer. The potential of the working electrode was typically decreased in 30 mV steps until the enzyme was fully reduced and increased stepwise until reoxidation was complete. After each step, the current and UV/vis absorption spectrum was monitored until no further change occurred. This equilibration process typically lasted 15 min. The Ag/AgCl reference electrode employed in the OTTLE cell was calibrated against indigotrisulfonic acid ($E_0' = -99$ mV vs SHE) and FMN ($E_0' = -220$ mV vs SHE) in the same buffer conditions and found to be +205 ± 2 mV relative to the standard hydrogen electrode (SHE). All electrode potentials have been corrected accordingly. Absorbance changes were plotted against the potential of the working electrode and analyzed by fitting absorbance data at one or more wavelengths simultaneously to a modified Nernst equation (eq 1) using Origin 7.0 (Microcal). nNOSFAD redox titrations were also conducted in the presence of equimolar amounts of ADP^+ and $NADP^+$. In the latter case, the data were analyzed with eq 2, which incorporates the additional $NADP^+$/NADPH 2 e^- redox couple (E_3'). The nNOSrd data were analyzed as described previously.[28]

$$\frac{a\log_{10}{}^{-1}\left(\frac{E-E_1'}{59}\right)+b+c\log_{10}{}^{-1}\left(\frac{E_2'-E}{59}\right)}{1+\log_{10}{}^{-1}\left(\frac{E-E_1'}{59}\right)+\log_{10}{}^{-1}\left(\frac{E_2'-E}{59}\right)} \quad (1)$$

where *a*, *b*, and *c* are the absorbances of oxidized flavin, flavin semiquinone, and hydroquinone, respectively, *E* is the potential of the working electrode, and E_1' and E_2' are the midpoint potentials of the oxidized flavin/semiquinone and semiquinone/hydroquinone redox couples (*28*). Parameters *a*, *b*, *c*, E_1', and E_2' are variables determined by least-squares fitting.

$$\left[a\log_{10}{}^{-1}\left(\frac{2E-E_1'-E_2'}{59}\right)+b\log_{10}{}^{-1}\left(\frac{E-E_2'}{59}\right)+c+d\log_{10}{}^{-1}\left(\frac{E_3'-E}{29.5}\right)\right]\Big/\left[1+\log_{10}{}^{-1}\left(\frac{2E-E_1'-E_2'}{59}\right)+\log_{10}{}^{-1}\left(\frac{E-E_2'}{59}\right)+\log_{10}{}^{-1}\left(\frac{E_3'-E}{29.5}\right)\right] \quad (2)$$

where *a*, *b*, *c*, and *d* are the absorbances of oxidized flavin, flavin semiquinone, flavin hydroquinone−$NADP^+$ charge-transfer complex, and flavin hydroquinone−NADPH complex, respectively, *E* is the potential of the working electrode, and E_1', E_2', and E_3' are the midpoint potentials of the oxidized flavin/semiquinone, semiquinone/hydroquinone−$NADP^+$ CT complex, and hydroquinone−$NADP^+$ CT complex/hydroquinone−NADPH complex redox couples, respectively. Parameters *a*, *b*, *c*, *d*, E_1', E_2', and E_3' are variables determined by least-squares fitting.

RESULTS

Preparation of nNOSFMNCaM. Neuronal NO synthase FMN-binding domain was coexpressed with calmodulin in *E. coli* and purified with CaM bound throughout. Removal of CaM at any stage during the purification procedure by addition of EGTA led to proteolysis of the domain, precipitation of the protein or both. Addition of the detergents Tween 20 and deoxycholate did not prevent this. Purification by DEAE and Q-sepharose anion-exchange chromatography and Superdex S200 gel filtration resulted in a 1:1 complex of nNOS FMN domain and Ca^{2+}-bound CaM with a purity of >90% as judged by SDS−PAGE (Figure 1). Typical yields were 10 mg of pure protein from 30 g of *E. coli*, wet weight. In the initial lysate, the nNOSFMNCaM complex was dark gray/blue, indicative of the stable semiquinone form. As the purification progressed, the FMN turned yellow as oxidation occurred. The blue-gray semiquinone was easily regenerated by addition of dithionite and remained in this oxidation state for several hours in the presence of air. Inclusion of 10 mM DTT in the buffers during purification was found to prevent oxidation; however, this was not necessary for the stability of the enzyme or its purification. Figure 1 shows an SDS−PAGE gel of purified nNOSFMNCaM; the bands observed at 28 and 16 kDa correspond to the masses of nNOS FMN domain (28 209 Da) and CaM (16 707 Da). The molar absorption coefficient of nNOSFMNCaM was determined to be 10 400 M^{-1} cm^{-1} at 457 nm for the oxidized enzyme and 4300 M^{-1} cm^{-1} at 592 nm for the semiquinone form.

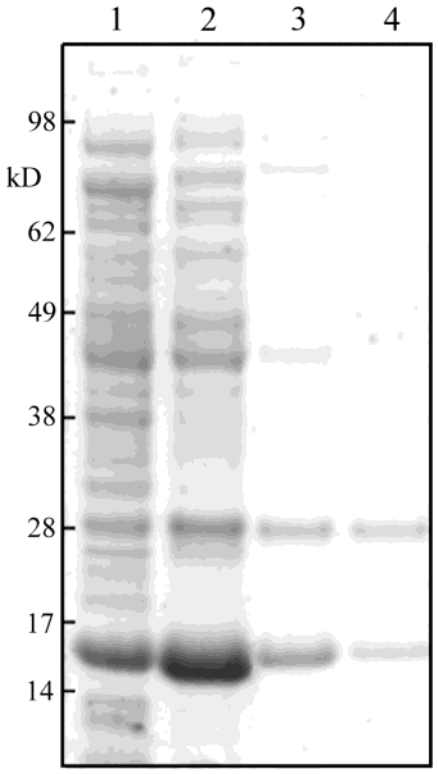

FIGURE 1: SDS−PAGE of nNOS FMN domain with bound CaM at different stages of purification: lane 1, cell lysate; lane 2, after DEAE Sephacel; lane 3, after Q-Sepharose FPLC; lane 4, after Superdex S200 FPLC.

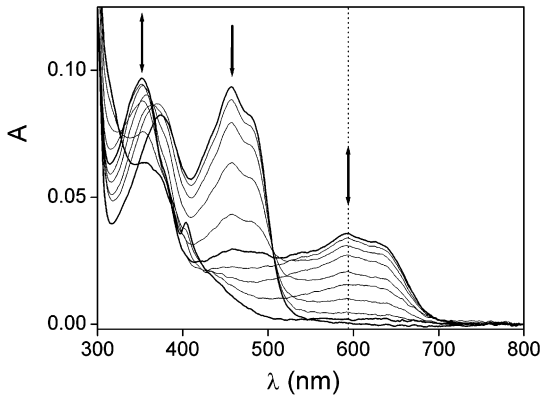

FIGURE 2: UV/visible spectra of nNOS FMN domain with bound CaM during spectroelectrochemical redox titration. nNOSFMNCaM (275 μM) was reduced electrochemically in 0.1 M Tris/HCl, pH 7.5, 0.5 M KCl at 25 °C with steps of −30 mV between each spectrum. Arrows indicate how the spectra change as reduction proceeds.

Spectroelectrochemical Analysis of nNOSFMNCaM. The midpoint potentials of the FMN/FMNH and $FMNH/FMNH_2$ redox couples of nNOSFMNCaM were determined using OTTLE potentiometry. Figure 2 shows the UV/vis spectrum of nNOSFMNCaM as it is reduced and oxidized stepwise in an OTTLE cell. The oxidized enzyme has absorbance maxima at 457 and 375 nm. These decay on reduction to the semiquinone form, which has absorbance maxima at 350 and 592 nm typical of the neutral blue FMN semiquinone formed by flavodoxin (*31*). Further reduction results in the disappearance of these bands. The two FMN redox couples were found to have fundamentally different electrochemical characteristics; this is illustrated in Figures 3 and 4. Typically,

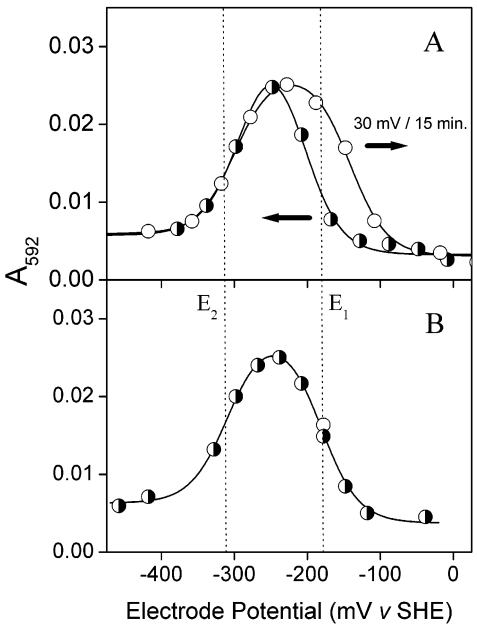

FIGURE 3: Determination of reduction potentials for nNOS FMN domain with bound CaM: (A) spectroelectrochemical titration with 20 min intervals between 40 mV redox steps in the reductive (◑) and oxidative (○) directions; (B) spectroelectrochemical titration with full equilibration after each redox step. Data are shown fitted to eq 1; the broken lines mark the midpoint potentials of the two FMN redox couples for the data in panel B.

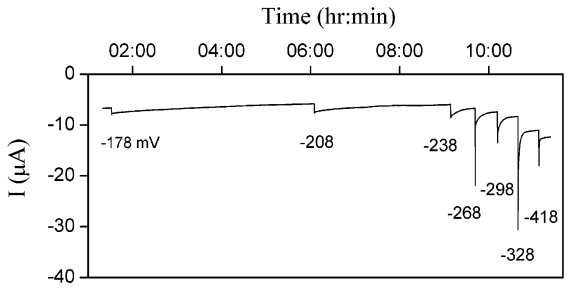

FIGURE 4: Spectroelectrochemical time-course for nNOS FMN domain with bound CaM. The current flowing between working and counter electrodes (*I*) is plotted against time. The potential of the working electrode was stepped down by 30 mV after each equilibration. Data relate to Figure 3, panel B.

after the potential of the working electrode is stepped by 30 mV, the resulting surge in current relaxes back to the base level within 10−15 min. Providing the concentration of enzyme and mediators are sufficient, the relaxation rate is limited by the conductivity of the solution as determined by the concentration of electrolyte present and the arrangement/dimensions of the cell. During both reduction and oxidation of the FMN through the oxidized flavin/semiquinone redox couple, a significant slowing of the equilibration process occurred. The semiquinone/hydroquinone redox couple, on the other hand, exhibited normal relaxation behavior. Figure 3 shows the results of two different spectroelectrochemical titrations. In Figure 3A, the absorbance due to semiquinone generated is plotted against reduction potential as the working electrode was stepped down by 30 mV at 15 min intervals until the FMN was fully reduced and then the process was reversed. While the semiquinone/hydroquinone couple was freely reversible, the oxidized flavin/semiquinone couple was observed to be severely hysteretical under these conditions with some 80 mV separating the forward and reverse redox transitions. In Figure 3B, a similar plot is shown in which the solution was left to equilibrate fully after each redox step. At the higher potentials, equilibration took place over as much as 5 h, that is, 20-fold more slowly than at low potentials. This is illustrated in Figure 4. The protracted relaxation of the current shown was accompanied by a slowly changing visible spectrum. The data plotted in Figure 3B were used to calculate the equilibrium reduction potentials of the two FMN redox couples; these were −179 mV for FMN/FMNH and −314 mV for FMNH/$FMNH_2$ (Table 1).

Spectroelectrochemical Analysis of nNOSFAD. The midpoint potentials of the oxidized flavin/semiquinone and semiquinone/hydroquinone redox couples of the nNOS FAD-binding subdomain were determined in the absence and presence of stoichiometric amounts of ADP and $NADP^+$. The enzyme and ligand concentrations in these experiments were 300−500 μM, which is well in excess of the K_I values of these inhibitors (*32*). They should therefore form 1:1 complexes (*33*). Figure 5A shows how the UV/visible spectrum of nNOSFAD changes during electrochemical reduction. The absorbance maximum at 460 nm decays rapidly during the early stages of reduction and a band at 597 nm appears, characteristic of a neutral blue semiquinone. This ultimately decays away as the FAD hydroquinone is formed. In Figure 5B, the absorbance at 460 nm and the difference in the absorbances at 650 and 700 nm are plotted against the corrected potential of the working electrode. The two sets of data were fitted simultaneously to eq 1 to give reduction potentials of −291 and −326 mV for the FAD/FADH and FADH/$FADH_2$ couples, respectively.

In the presence of $NADP^+$, there were significant differences in both the UV/vis spectra of intermediates formed during reduction (Figure 6) and the final reduction potentials determined. As the nNOSFAD−$NADP^+$ complex was reduced, the 460 nm band disappeared and the neutral, blue FAD semiquinone appeared (at 697 nm), as observed for the uncomplexed enzyme (Figure 6A). However, further reduction resulted in the appearance of a broad absorbance band at 780 nm, characteristic of a $FADH_2$−$NADP^+$ charge-transfer complex. $NADP^+$ is the product of NADPH dehydrogenation at the FAD site of nNOS and is known to form a charge-transfer complex with the FAD hydroquinone as the nicotinamide and isoallaxazine rings stack above one another (*32*−*34*). At lower potentials, the charge-transfer complex was reduced, resulting in the formation of the $FADH_2$−NADPH complex and loss of the charge-transfer band. Formation of NADPH was accompanied by an increase in absorbance at 355 nm (Figure 6). The absorbance at 355 nm is the approximate position of an isosbestic point in the nNOSFAD redox titration and is mainly influenced by changes in the relative concentrations of $NADP^+$ and NADPH. Absorbance changes at 460 nm are mainly due to the disappearance of oxidized FAD. The $\Delta A_{650-700}$ (difference in the absorbances at 650 and 700 nm) indicates the formation and decay of FAD semiquinone (the subtraction minimizes contributions from the charge-transfer complex), and the absorbance at 780 nm is due to the FADH−$NADP^+$ charge-transfer complex. In Figure 6B, all these values are plotted against the potential of the working electrode. Together they indicate how the concentrations of each of the four redox states (FAD−$NADP^+$, FADH−$NADP^+$, $FADH_2$−$NADP^+$, $FADH_2$−NADPH) vary with potential.

Table 1: Reduction Potentials of the FMN, FAD, and $NADP^+$ Cofactors of nNOSrd, nNOSFMNCaM, and nNOSFAD[a]

	redox couple					
	FMN/H[b]	FMNH/H_2[c]	FAD/H[b]	FADH/H_2[c]	NADP/H[d]	heme[e] $Fe^{III/II}$
nNOSrd + CaM[f]	-98 ± 5	-300 ± 8	-296 ± 6	-320 ± 10		
nNOSFMNCaM	-179 ± 3	-314 ± 3				
nNOSFAD			-291 ± 3	-326 ± 3		
nNOSFAD + ADP[f]			-297 ± 6	-323 ± 7		
nNOSFAD + $NADP^+$[f]			-304 ± 5	-290 ± 5	-356 ± 3	
free $NADP^+$[d]					-332[d]	
nNOS heme domain[e]						-306[e]

[a] Measurements were taken at 25 ± 1 °C in 100 mM Tris/HCl buffer, pH 7.5, 0.5 M KCl. [b] Reduction potential of the flavin oxidized/semiquinone redox couple. [c] Reduction potential of the flavin semiquinone/hydroquinone redox couple. [d] Reduction potential of the $NADP^+$/NADPH two-electron redox couple adjusted by 30 mV per pH unit (*29*). [e] Reduction potential of the isolated nNOS oxygenase domain heme Fe^{III}/Fe^{II} redox couple in the presence of L-arginine (*30*) repeated under above conditions. [f] In the presence of stoichiometric amounts of bound CaM, ADP, and $NADP^+$, respectively.

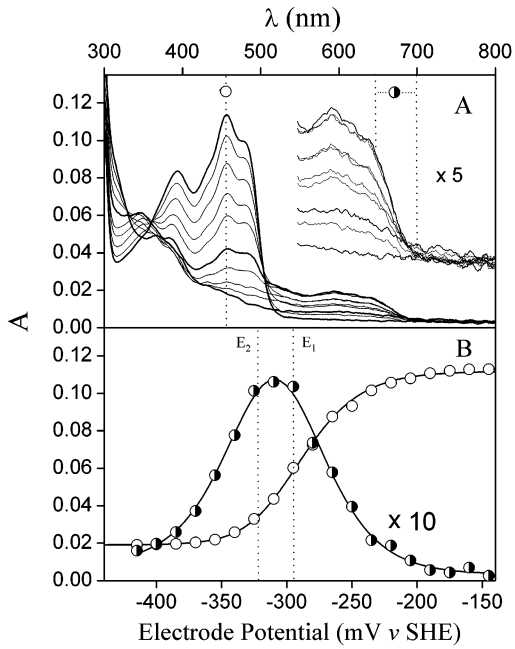

FIGURE 5: Determination of reduction potentials for nNOSFAD: (A) UV/vis spectra collected during spectroelectrochemical titration of 300 μM enzyme in 100 mM Tris/HCl, pH 7.5, 0.5 M KCl at 25 °C; (B) plot of electrode potential vs absorbance at 460 nm (○) and the difference in the absorbances at 650 and 700 nm (◑) fitted simultaneously to eq 1.

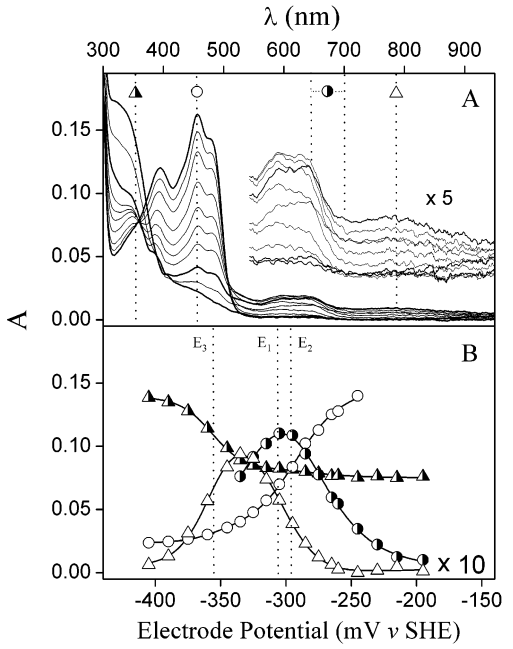

FIGURE 6: Determination of reduction potentials for nNOSFAD in the presence of $NADP^+$: (A) UV/vis spectra collected during spectroelectrochemical titration of 300 μM enzyme and $NADP^+$ (1:1 complex) in 100 mM Tris/HCl, pH 7.5, 0.5 M KCl at 25 °C; (B) plot of electrode potential vs absorbance at 355 nm (▲), 460 nm (○), and 780 nm (△) and the difference in the absorbances at 650 and 700 nm (◑) fitted simultaneously to eq 2.

The data were fitted simultaneously to eq 2 to give equilibrium reduction potentials for the three transitions (Table 1). The data were also used to calculate the molar absorption coefficient for the FADH−$NADP^+$ charge-transfer complex at the absorption maximum of 780 nm to be 970 M^{-1} cm^{-1}. The molar absorption coefficient for the oxidized isolated FAD domain used in this calculation was determined to be 10 560 M^{-1} cm^{-1} at the absorption maximum of 456 nm.

The presence of ADP had much less influence on the UV/vis spectra of the different nNOSFAD redox species (Figure 7). The proportion of semiquinone generated during the redox titration was less than that for the uncomplexed enzyme but was more than that in the presence of $NADP^+$. No charge-transfer species were observed. In Figure 7B, the absorbance at 460 nm and the difference in absorbance at 650 and 700 nm are plotted against the potential of the working electrode. The data were fitted to eq 1. In this case, the semiquinone absorbance parameter was fixed to the same value obtained in the absence of ADP (which was the same as that obtained in the presence of $NADP^+$). Fixing this parameter is likely to give better consistency because the extinction coefficient is unlikely to change much in the presence of the inhibitor (it is otherwise spectroscopically identical). The error margins given in Table 1 reflect the uncertainty in this value. ADP appeared to affect the oxidized FAD/semiquinone redox couple, disfavoring semiquinone formation slightly. Although it is clear that there is slightly less semiquinone formed during this redox titration, the shifts in potential observed are similar to the experimental errors.

The nNOSFAD redox titrations were all freely reversible with no hysteresis observed in any of the redox couples.

Spectroelectrochemical Analysis of nNOS Reductase Domain. OTTLE cell potentiometric titration of nNOSrd (not shown) was conducted under the same conditions as used for the subdomains above (0.1 M Tris/HCl, pH 7.5, 0.5 M KCl). The changes in UV/vis spectrum observed closely

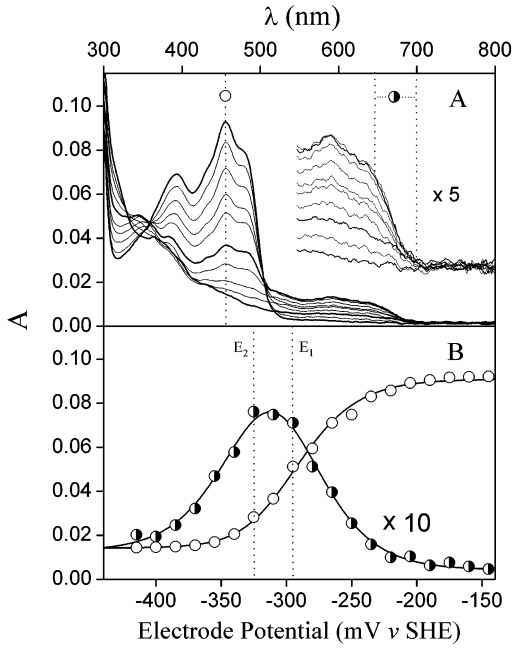

FIGURE 7: Determination of reduction potentials of nNOSFAD in the presence of ADP: (A) UV/vis spectra collected during spectroelectrochemical titration of 300 μM enzyme and ADP (1:1 complex) in 100 mM Tris/HCl, pH 7.5, 0.5 M KCl at 25 °C; (B) plot of electrode potential vs absorbance at 460 nm (○) and the difference in the absorbances at 650 and 700 nm (◑) fitted simultaneously to eq 1.

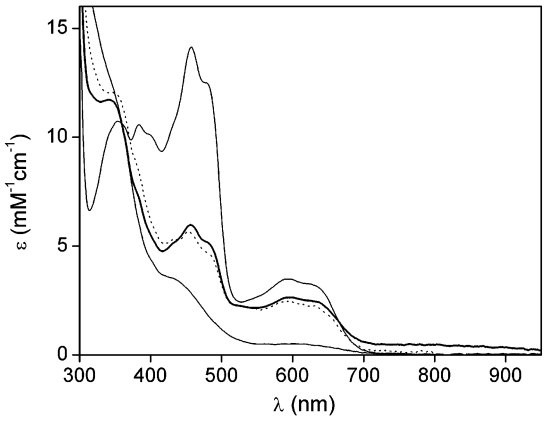

FIGURE 8: UV/vis absorbance spectra of nNOSrd during electrochemical reduction. The solid thin lines are the oxidized (with stable FMN semiquinone) and fully reduced spectra from electrochemical reduction of nNOSrd. The solid thick line is the spectrum of $NADP^+$-bound nNOSrd with maximum charge-transfer band. The dotted line is unbound nNOSrd at a similar stage of reduction. All spectra were recorded in 100 mM Tris/HCl, pH 7.5, 0.5 M KCl at 25 °C.

matched those reported previously (*17*) using chemical reduction/oxidation in 0.05 M Tris/HCl, pH 7.1, 0.1 M KCl. The data (see Table 1) were fitted in a similar way, using absorption coefficients calculated for the separate domains (above) and show a broad shift in potential of 30−60 mV largely attributable to the increase in pH. The results are useful for comparison with the subdomains and show how their separation affects the properties of the FMN and FAD cofactors. The only significant difference is in the potential of the FMN/FMNH redox couple, which is 80 mV higher in nNOSrd than in the isolated FMN−CaM domain. This indicates that contacts between the two subdomains are important for controlling the environment of the FMN cofactor. The experiment with nNOSFAD was repeated in the presence of a stoichiometric amount of $NADP^+$, which produced a charge-transfer complex with similar spectral characteristics (i.e., band position and intensity) to that observed with the isolated FAD domain (Figure 8). Fitting of the electrochemical data obtained was abandoned due to the complexity of the system, which has five separate redox couples. However, the data appeared to be consistent with the behavior of the $NADP^+$-free enzyme and $NADP^+$-bound nNOSFAD in the analogous experiments.

DISCUSSION

Electron transfer through neuronal NO synthase is controlled by a remarkable series of structural features and ligands. These include autoinhibitory domains and the reversible ligation of calmodulin (CaM) and inhibitor proteins (*13*, *14*, *18*−*23*, *37*). The reductase domain of nNOS is considered to be catalytically repressed in the absence of CaM with both reduction and oxidation of the flavins being affected. However, attempts to determine which individual catalytic steps repress electron transfer through nNOSrd have resulted in controversy with electron transfer (*36*, *38*, *39*), hydride transfer (*15*), and product dissociation (*24*, *36*) all being suggested.

It has recently been shown that the conformation of nNOSrd is dependent on NADP/H binding (*24*) and that in the holoenzyme, the FAD-stacking residue (F1395) helps to regulate electron transfer from the reductase domain to heme (*25*). The possibility that the conformation of the reductase domain, NADP/H binding, or both influence the redox properties of the flavin cofactors and therefore the electron transfer steps was assessed by studying the separate FMN- and FAD-binding subdomains. The FMN domain (nNOSFMNCaM) was found to be stable only in the presence of bound CaM/Ca^{2+}, preventing analysis of the CaM-free form. The FMN cofactor formed a stable blue semiquinone, which oxidized slowly in air, much like the FMN semiquinone formed in nNOS holoenzyme and in the reductase domain (nNOSrd). However, the reduction potential for the FMN oxidized/semiquinone redox couple was 80 mV lower than that in nNOSrd. This indicates that the FAD-domain has a large influence on the environment of the FMN and acts to stabilize the semiquinone thermodynamically. This effect was not observed with the related enzymes human CPR (*44*) and methionine synthase reductase (*45*). The same redox couple was also found to exhibit strong hysteresis during electrochemical reduction and oxidation, as shown in Figures 3 and 4. By analogy with related flavodoxins, the cause of this effect is likely to be a hydrogen bonding interaction between the peptide carbonyl of Gly810 and the flavin N5, which is protonated in the semiquinone form but not in the oxidized form (*31*). The result is a kinetically stable semiquinone, which does not oxidize during the normal catalytic turnover of nNOS. The FMN sq/hq redox couple is, however, the same in both nNOSFMNCaM and nNOSrd. This redox couple is freely reversible and is utilized in the transfer of electrons from FAD to heme in nNOS. The FAD-domain, therefore, appears to have little influence on the potential of the viable electron on the FMN cofactor. Given this, it also seems unlikely that the conformation of the FAD domain

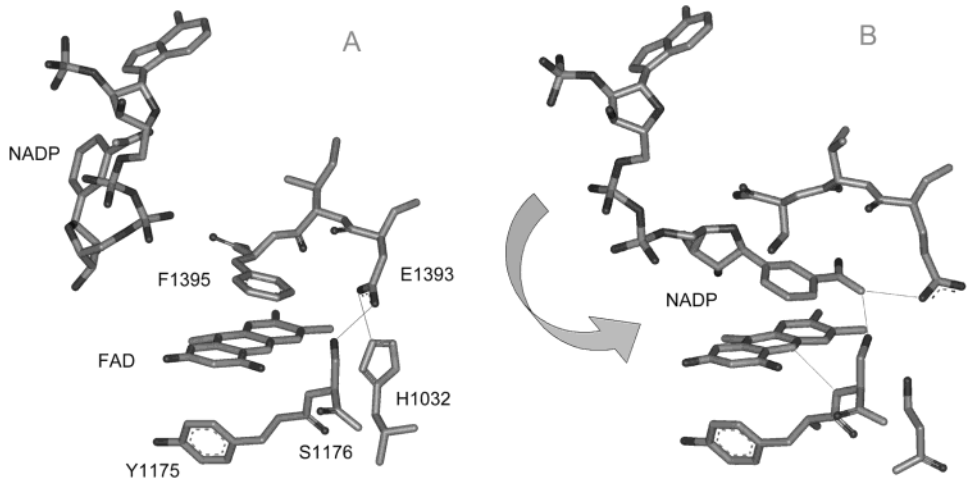

FIGURE 9: The active sites of nNOS FAD domain (A) (*10*) and ferredoxin reductase Y308S mutant (B) (*32*) with $NADP^+$ bound.

could affect the reduction potential of the FMN sq/hq couple. The kinetic and thermodynamic stability of the FMN semiquinone toward oxidation ensures that the FMN cofactor acts only as a one-electron donor. This is likely to be important to the mechanism of nitric oxide synthesis, which requires the delivery of single electrons at an optimum rate. According to the kinetic model defined by Santolini et al., (*40*) transfer of electrons pairwise to the heme would result in a build up of stabilized ferrous NO complex during turnover, which would ultimately slow the overall rate of catalysis.

The reduction potentials of the FAD cofactor were also found to be unchanged in the isolated nNOS FAD domain, indicating that the FMN domain has little effect on the redox properties of this cofactor. It seems unlikely, therefore, that the conformation of the reductase domain alone could control the driving force for electron transfer through the flavins. This is consistent with the fact that CaM binding has little effect on the flavin reduction potentials (*17*). Substrate ($NADP^+$) binding, however, was found to stabilize the hydroquinone form of the FAD, by increasing the reduction potential of the sq/hq couple by 30−40 mV. Some destabilization of the semiquinone also occurred, as indicated by a decrease in the potential of the ox/sq couple. The inhibitor ADP did not cause stabilization of the FAD-hydroquinone, suggesting that interactions between the nicotinamide substituent (NMN) and the reduced enzyme are responsible for the effect. The most likely cause is a favorable interaction between the oxidized NMN and the FAD hydroquinone, which form a π-stacked charge-transfer complex. Similar complexes are formed by the nNOSFAD and nNOSrd constructs as shown in Figures 6 and 8 and have been characterized for the related enzymes P450 reductase (CPR) (*41*) and ferredoxin reductase (FNR) among others (*34*). For FNR, it has also been shown that the two-electron reduction potential of the FAD/$NADP^+$ system increases on formation of a charge-transfer complex, although in this case the $NADP^+$ is preferentially reduced rather than the FAD. This is due to a more negative FAD reduction potential in FNR, which generally operates in the reverse direction to nNOSFAD, catalyzing NADPH formation rather than dehydrogenation (*34*). The X-ray crystal structure of the nNOSFAD construct (*10*) shows the FAD π-stacked with the F1395 residue (Figure 9); this must move for hydride transfer to occur from NADPH, which is shown bound in a nonproductive conformation. The analogous residues in FNR and CPR are Y308 and W677, respectively. The X-ray structures of the Y308S mutant of FNR (*35*) and the W677G mutant of CPR (*43*) show the NMN substituent stacked with the FAD in a productive conformation. Figure 9 illustrates the conformational change required for the NADPH to initiate hydride transfer. Substantial movement of the active site residues must also occur during this process; however, these cannot be predicted from the mutant structure. The nonproductive conformation of bound $NADP^+$ appears to be dominant for NOS, FNR, and CPR. This stems from the high affinity of the enzymes for the ADP substituent of the substrate, which guarantees a low K_d, and negative binding affinity for the NMN group, as demonstrated for CPR (*42*). It has therefore been proposed that the stacking residue acts to dislodge the NMN group from the FAD as part of the catalytic process. Mutants lacking a bulky aromatic at this position bind NADP(H) more tightly and are catalytically limited by product dissociation. The charge-transfer complex formed by the CPR FAD domain W676 mutant and NADPH was found to be particularly stable, releasing $NADP^+$ at a much lower rate (*41*). Recent evidence also suggests a link between the conformation of bound NADP(H), the FAD-stacking residue, and the accessibility of the FMN to external electron acceptors (e.g., the oxygenase domain and cytochrome *c*) in nNOS. We can now add that the conformation of the $NADP^+$ is also likely to affect the reduction potentials of the FAD, assuming the π-stacking interaction is responsible for the shifts observed in the presence of $NADP^+$. Therefore, with bound $NADP^+$, the conformation of the three-electron reduced nNOS reductase domain may influence the equilibrium distribution of electrons in the FAD and FMN cofactors and vice versa. The shift in the FAD sq/hq potential observed is only 30−40 mV, which would be too small to have a significant effect on overall catalytic rate constants. However, this shift is averaged over all the conformations existing at equilibrium and takes no account of the proportion of enzyme molecules with NMN and FAD in the stacked conformation.

Scheme 1 shows a simple model describing the $NADP^+$-bound FAD sq/hq redox couple. The nNOSFAD is assumed to exist in two conformations, which are roughly assigned to the π-stacked and unstacked conformations depicted in

Scheme 1

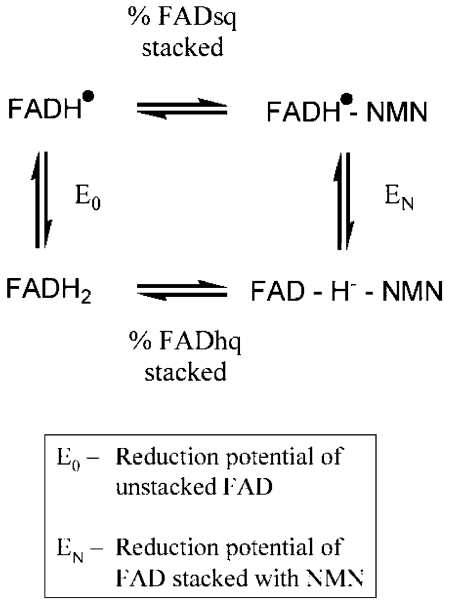

Figure 9. The unstacked reduction potential is given by E_0 (−323 mV, i.e., ADP-bound nNOSFAD) and the reduction potential of fully π-stacked enzyme is given by E_N. The reduction potential shift observed experimentally (33 mV) is dependent on the value of E_N and the proportions of π-stacked FAD hydroquinone and semiquinone at equilibrium. All of these are unknown. The relationships among the three unknowns can be modeled using the Nernst equation and Scheme 1 to produce the plot in Figure 10. The plot shows that E_N can be any value lower than the experimentally observed reduction potential in the presence of $NADP^+$ (−290 mV) but that the π-stacking coefficients are limited to greater than 70% for the hydroquinone and less than 30% for the semiquinone. The π-stacking interaction is likely to be dependent on the redox state of the FAD. Electrostatics, hydrogen bonding, and electronic interactions may all be involved in defining the energy of interaction. The high value for the hydroquinone compared to the semiquinone suggests that the effect is electronic, perhaps benefiting from the same factors stabilizing the transition state of the active hydride-transfer complex. Parallels can be drawn with FNR and CPR. Deng et al. (*35*) calculated that for wild-type FNR π-stacking between bound $NADP^+$ and oxidized FAD was approximately 10% on the basis of spectral changes. The magnitude of the charge-transfer band formed by the FAD hydroquinone of wild-type FNR and bound $NADP^+$ (*34*) indicates that a much larger proportion lies in the π-stacked conformation, as compared to the charge-transfer band formed by the Y308S mutant.

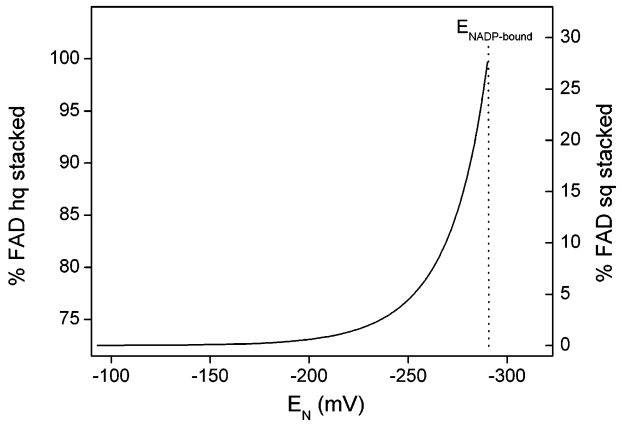

FIGURE 10: A simulation showing the dependence of nicotinamide−FAD stacking in the nNOS FAD domain on the sq/hq reduction potential of the stacked form. The model assumes that the bound $NADP^+$ has two distinct conformations (stacked/unstacked) as in Figure 8 and that the unstacked form has the same reduction potential as the ADP-bound enzyme ($E_0 = -323$ mV). E_N is the reduction potential of the stacked form (as in Scheme 1) and $E_{NADP-bound}$ is the experimentally determined reduction potential of the substrate-bound enzyme.

Given the available evidence, it is impossible to say exactly what the π-stacking coefficients are or what the value of E_N is in Figure 10. However, if the FAD semiquinone is unable to form energetically favorable π-stacked complexes with the NMN, it is possible that E_N lies in the −200 to −250 mV range. This would influence the equilibrium distribution of electrons between the FAD and FMN, particularly for the three-electron reduced enzyme form, such that when the $NADP^+$ is in the stacked conformation, the FAD hydroquinone would be favored, preventing formation of FMN hydroquinone. In the unstacked conformation, the reverse would be true. Addition of NADPH to fully reduced nNOSrd causes the enzyme to adopt a conformation in which the FMN hydroquinone is inaccessible to the external electron acceptor, cytochrome *c* (*24*). It is likely that the NADPH adopts an unstacked conformation in this case, since formation of a charge-transfer complex between the two reduced nucleotides is improbable. If the π-stacked NADP(H) conformation corresponds with the open enzyme conformation, it may be that electron transfer from nNOSrd is inhibited by a FAD−NADPH reduction potential switch in this conformation and by inaccessibility of the FMN in the other conformation (with unstacked $NADP^+$). Since CaM binding relieves conformational restriction of nNOSrd, this would activate electron transfer through the enzyme.

In a recent report by Dunford et al. (*46*), the potentials of the FAD in an isolated FAD-domain construct were reported to be markedly different: −177 mV for the oxidized FAD/semiquinone and −310 mV for the semiquinone/hydroquinone couples (at pH 7). However, the data are of poor quality and appear to have been analyzed inappropriately. These potentials would result in almost total FAD semiquinone formation at the reduction midpoint, yet it is clear from the spectra presented that this is not the case. Mutation of the FAD-stacking residue F1395 to serine is also reported in the paper to have little effect on the FAD reduction potentials, although the spectral data show that much less semiquinone (20−30%) is formed during reductive titration of the mutant enzyme, indicating a divergence in the two potentials of more than 60 mV favoring hydroquinone formation.

CONCLUSIONS

The reduction potentials of the FAD/FADH, FADH/$FADH_2$, FMNH/$FMNH_2$, and heme Fe^{III}/Fe^{II} redox couples for the isolated nNOS domains all lie within a 30 mV range in the presence or absence of substrates. This facilitates efficient electron transfer through the enzyme and ensures that all these redox states are populated at equilibrium. The FMN semiquinone was found to be kinetically and thermo-

dynamically stabilized toward oxidation, although the thermodynamic stability was greater in the presence of the FAD domain. $NADP^+$ was found to induce a modest shift in the FADH/$FADH_2$ redox couple from −326 to −290 mV, probably induced by the formation of a π-stacked charge-transfer complex. The significance of this effect is dependent on the relationship between the enzyme conformation and the fraction of bound $NADP^+$ molecules adopting the π-stacked conformation. It is possible that electron transfers between both FAD and FMN and FMN and heme are influenced by the conformation of bound $NADP^+$, which may act to inhibit electron flow through nNOS in the absence of CaM. Further studies are required to determine whether the shift in the FAD reduction potential is tightly coupled to conformational changes and whether the resulting electron redistribution is enough to inhibit electron transfer from FMN to heme in the CaM-free enzyme under turnover conditions.

ACKNOWLEDGMENT

The authors would like to thank J. G. Guillemette for supplying the nNOSrd expression plasmid.

REFERENCES

1. Mayer, B., Ed. (2000) *Nitric Oxide, Handbook of Experimental Pharmocology*; Vol. 143, Springer-Verlag, Berlin.
2. Ignarro, L. J., Ed. (2000) *Nitric Oxide: Biology and Pathobiology*, Academic Press, San Diego, CA.
3. Stuehr, D. J. (1999) Mammalian nitric oxide synthases, *Biochim. Biophys. Acta 1411* 217−230.
4. Alderton, W. K., Cooper, C. E., and Knowles, R. G. (2001) Nitric oxide synthases: structure, function and inhibition, *Biochem. J. 357*, 593−615.
5. Crane, B. R., Arvai, A. S., Ghosh, D. K., Wu, C., Getzoff, E. D., Stuehr, D. J., and Tainer, J. A. (1998) Structure of nitric oxide synthase oxygenase dimer with pterin and substrate, *Science 279*, 2121−2126.
6. Raman, C. S., Li, H., Martasek, P., Kral, V., Masters, B. S. S., and Poulos, T. L. (1998) Crystal structure of constitutive endothelial nitric oxide synthase: A paradigm for pterin function involving novel a metal center, *Cell 95*, 939−950.
7. Siddhanta, U., Presta, A., Fan, B. C., Wolan, D., Rousseau, D. L., and Stuehr, D. J. (1998) Domain swapping in inducible nitric oxide synthase − Electron transfer occurs mainly between flavin and heme groups located on adjacent subunits in the dimer, *J. Biol. Chem. 273*, 18950−18958.
8. Sagami, I., Daff, S., and Shimizu, T. (2001) Intrasubunit and Intersubunit Electron Transfer in Neuronal Nitric-oxide Synthase: Effect of Calmodulin on Heterodimer Catalysis, *J. Biol. Chem. 276*, 30036−30042.
9. Wang, M., Roberts, D. L., Paschke, R., Shea, T. M., Masters, B. S. S., and Kim, J. P. (1997) Three-dimensional structure of NADPH-cytochrome P450 reductase: prototype for FMN- and FAD-containing enzymes, *Proc. Natl. Acad. Sci. U.S.A. 94*, 8411−8416.
10. Zhang, J., Martasek, P., Paschke, R., Shea, T. M., Masters, B. S. S., and Kim, J. P. (2001) Crystal structure of the FAD/NADPH-binding domain of rat neuronal nitric oxide synthase − Comparisons with NADPH-cytochrome P450 oxidoreductase, *J. Biol. Chem. 276*, 37506−37513.
11. Bredt, D. S., Hwang, P. M., Glatt, C. E., Lowenstein, C., Reed, R. R., and Snyder, S. H. (1991) Cloned and expressed nitric oxide synthase structurally resembles cytochrome P450 reductase, *Nature 351*, 714−718.
12. Masters, B. S. S. (1994) Nitric oxide synthases − why so complex, *Annu. Rev. Nutr. 14*, 131−145.
13. Abu-Soud, H. M., and Stuehr, D. J. (1993) Nitric-oxide synthases reveal a role for calmodulin in controlling electron transfer, *Proc. Natl. Acad. Sci. U.S.A. 90*, 10769−10772.
14. Abu-Soud, H. M., Yoho, L. L., and Stuehr, D. J. (1994) Calmodulin controls neuronal nitric oxide synthase by a dual mechanism − Activation of intradomain and interdomain electron-transfer, *J. Biol. Chem. 269*, 32047−32050.
15. Gachhui, R., Presta, A., Bentley, D. F., Abu-Soud, H. M., McArthur, R., Brudvig, G., Ghosh, D. K., and Stuehr, D. J. (1996) Overexpression and characterization of the neuronal NO synthase flavoprotein domain, *J. Biol. Chem. 271*, 20594−20602.
16. Sheta, E. A., McMillan, K., and Masters, B. S. S. (1994) Evidence for a bidomain structure of constitutive cerebellar nitric oxide synthase, *J. Biol. Chem. 269*, 15147−15153.
17. Noble, M. A., Munro, A. W., Rivers, S. L., Robledo, L., Daff, S. N., Yellowlees, L. J., Shimizu, T., Sagami, I., Guillemette, J. G., and Chapman, S. K. (1999) Potentiometric Analysis of the Flavin Cofactors of Neuronal Nitric Oxide Synthase, *Biochemistry 38*, 16413−16418.
18. Roman, L. J., Martasek, P., and Masters, B. S. S. (2002) Intrinsic and Extrinsic Modulation of Nitric Oxide Synthase Activity, *Chem. Rev. 102*, 1179−1189.
19. Salerno, J. C., Harris, D. E., Irizarry, K., Patel, B., Morales, A. J., Smith, S. M. E., Martasek, P., Roman, L. J., Masters, B. S. S., Jones, C. L., Weissman, B. A., Lane, P., Liu, Q., and Gross, S. S. (1997) An autoinhibitory control element defines calcium-regulated isoforms of nitric oxide synthase, *J. Biol. Chem. 272*, 29769−29777.
20. Nishida, C. R., and Ortiz de Montellano, P. R. (1999) Autoinhibition of endothelial nitric oxide synthase − Identification of an electron-transfer control element, *J. Biol. Chem. 274*, 14692−14698.
21. Daff, S., Sagami, I., and Shimizu, T. (1999) The 42-Amino Acid Insert in the FMN Domain of Neuronal Nitric Oxide Synthase Exerts Control over Ca^{2+}/Calmodulin-dependent Electron Transfer, *J. Biol. Chem. 274*, 30589−30595.
22. Roman, L. J., Miller, R. T., De la Garza, M. A., Kim, J. P., and Masters, B. S. S. (2000) The C-terminus of mouse macrophage inducible nitric oxide synthase attenuates electron flow through the flavin domain, *J. Biol. Chem. 275*, 21914−21919.
23. Roman, L. J., Martásek, P., Miller, R. T., Harris, D. E., De la Garza, M. A., Shea, T. M., Kim, J. P., and Masters, B. S. S. (2000) The C-termini of constitutive nitric oxide synthases control electron flow through the flavin and heme domains and affect modulation by calmodulin, *J. Biol. Chem. 275*, 29225−29232.
24. Craig, D. H., Chapman, S. K., and Daff, S. (2002) Calmodulin activates electron transfer through neuronal nitric-oxide synthase reductase domain by releasing an NADPH-dependent conformational lock, *J. Biol. Chem. 277*, 33987−33994.
25. Adak, S., Sharma, M., Meade, A. L., and Stuehr, D. J. (2002) A conserved flavin-shielding residue regulates NO synthase electron transfer and nicotinamide coenzyme specificity, *Proc. Natl. Acad. Sci. U.S.A. 99*, 13516−13521.
26. Newton, D. C., Montgomery, H. J., and Guillemette, J. G. (1998), The reductase domain of the human inducible nitric oxide synthase is fully active in the absence of bound calmodulin, *Arch. Biochem. Biophys. 359*, 249−257.
27. Ost, T. W. B., Clark, J., Mowat, C. G., Miles, C. S., Walkinshaw, M. D., Reid, G. A., Chapman, S. K., and Daff, S. (2003) Oxygen activation and electron transfer in Flavocytochrome P450 BM3, *J. Am. Chem. Soc. 125*, 15010−15020.
28. Daff, S. N., Chapman, S. K., Turner, K. L., Holt, R. A., Govindaraj, S., Poulos, T. L., and Munro, A. W. (1997) Redox Control of the Catalytic Cycle of flavocytochrome P450−BM3, *Biochemistry 36*, 13816−13823.
29. Clark, W. M. (1960) *Oxidation−Reduction Potentials of Organic Systems*, p 363, Williams and Wilkins, Baltimore, MD.
30. Presta, A., Weber-Main, A. M., Stankovich, M. T., and Stuehr, D. J. (1998) Comparative Effects of Substrates and Pterin Cofactor on the Heme Midpoint Potential in Inducible and Neuronal Nitric Oxide Synthases, *J. Am. Chem. Soc. 120*, 9460−9465.
31. Mayhew, S. G., and Tollin, G. (1992) General Properties of Flavodoxins, in *Chemistry and Biochemistry of Flavoenzymes* (Muller, F., Ed.) Vol. 3, pp 390−417, CRC Press, Boca Raton, FL.
32. Wolthers, K. R., and Schimerlik, M. I. (2001), Reaction of Neuronal Nitric Oxide Synthase with 2,6-Dichloroindolphenol and cytochrome *c*: Influence of the Electron Acceptor and Binding of Ca^{2+}-Activated Calmodulin on the Kinetic Mechanism, *Biochemistry 40*, 4722−4737.
33. Daff, S. (2004) An appraisal of multiple NADPH Binding-site Models Proposed for Cytochrome P450 Reductase, NO Synthase, and Related Diflavin Reductase Systems, *Biochemistry*, in press.

34. Batie, C. J., and Kamin, H. (1986) Association of ferredoxin-NADP+ reductase with NADP(H). Specificity and oxidation−reduction properties, *J. Biol. Chem. 261*, 11214−11223.
35. Deng, Z., Aliverti, A., Zanetti, G., Arakaki, A. K., Ottado, J., Orellano, E. G., Calcaterra, N. B., Ceccarelli, E. A., Carrillo, N., and Karplus, P. A. (1999) A productive NADP+ binding mode of ferredoxin-NADP + reductase revealed by protein engineering and crystallographic studies, *Nat. Struct. Biol. 6*, 847−853.
36. Knight, K., and Scrutton, N. S. (2002) Stopped-flow Kinetic Studies of Electron Transfer in the Reductase Domain of Neuronal Nitric Oxide Synthase: Reevaluation of the Kinetic Mechanism Reveals New Enzyme Intermediates and Variation With Cytochrome P450 Reductase, *Biochem. J. 367*, 19−30.
37. Nedvetsky, P. I., Sessa, W. C., and Schmidt, H. H. H. W. (2002) There's NO binding like NOS binding: Protein−protein interactions is NO/cGMP signaling, *Proc. Natl. Acad. Sci. U.S.A. 99*, 16510−16512.
38. Guan, Z.-W., Kamatani, D., Kimura, S., and Iyanagi, T. (2003) Mechanistic studies on the intramolecular one-electron transfer between the two flavins in the human neuronal nitric oxide synthase and inducible nitric oxide synthase flavin domains, *J. Biol. Chem. 278*, 30859−30868.
39. Guan, Z.-W., and Iyanagi, T. (2003), Electron transfer is activated by calmodulin in the flavin domain of human neuronal nitric oxide synthase, *Arch. Biochem. Biophys. 412*, 65−76.
40. Santolini, J., Adak, S., Curran, C. M. L., and Stuehr, D. J. (2001) A Kinetic Simulation Model That Describes Catalysis and Regulation in Nitric-oxide Synthase, *J. Biol. Chem. 276*, 1233−1243.
41. Gutierrez, A., Doehr, O., Paine, M., Wolf. C. R., Scrutton, N. S., and Roberts, G. C. K. (2000) Trp-676 facilitates nicotinamide coenzyme exchange in the reductive half-reaction of human cytochrome P450 reductase: properties of the soluble W676H and W676A mutant reductases, *Biochemistry 39*, 15990−15999.
42. Murateliev, M. B., and Feyereisen, R. (2000) Interaction of NADP-(H) with Oxidized and Reduced P450 Reductase during Catalysis. Studies with Nucleotide Analogues, *Biochemistry 39*, 5066−5074.
43. Hubbard, P. A., Shen, A. L., Paschke, R., Kasper, C. B., and Kim, J. J. P. (2001) NADPH−Cytochrome P450 Oxidoreductase Structural Basis for Hydride and Electron Transfer, *J. Biol. Chem. 276*, 29163−29170.
44. Munro, A. W., Noble, M. A., Robledo, L., Daff, S. N., and Chapman, S. K. (2001) Determination of the redox properties of human NADPH-cytochrome P450 reductase, *Biochemistry 40*, 1956−1963.
45. Wolthers, K. R., Basran, J., Munro, A. W., and Scrutton, N. S. (2003) Molecular dissection of human methionine synthase reductase: determination of the flavin redox potentials in full-length enzyme and isolated flavin-binding domains, *Biochemistry 42*, 3911−3920.
46. Dunford, A. J., Marshall, K. R., Munro, A. W., and Scrutton, N. S. (2004) Thermodynamic and kinetic analysis of the isolated FAD domain of rat neuronal nitric oxide synthase altered in the region of the FAD shielding residue Phe1395, *Eur. J. Biochem. 271*, 2548−2560.

BI049312V